Three-Dimensional Biofilm Model With Individual Cells and Continuum EPS Matrix

Erik Alpkvist,[1] Cristian Picioreanu,[2] Mark C.M. van Loosdrecht,[2] Anders Heyden[1]

[1]Applied Mathematics Group, School of Technology and Society, Malmö University, Östra/Stora Varvsgatan 11H, Malmö, SE-205 06 Sweden
[2]Department of Biotechnology, Faculty of Applied Sciences, Delft University of Technology, Julianalaan 67, 2628 BC Delft, The Netherlands; telephone: +31 15 2781551; fax: +31 15 2782355; e-mail: C.Picioreanu@tudelft.nl

Received 10 December 2005; accepted 6 March 2006

Published online 13 April 2006 in Wiley InterScience (www.interscience.wiley.com). DOI: 10.1002/bit.20917

Abstract: An innovative type of biofilm model is derived by combining an individual description of microbial particles with a continuum representation of the biofilm matrix. This hybrid model retains the advantages of each approach, while providing a more realistic description of the temporal development of biofilm structure in two or three spatial dimensions. The general model derivation takes into account any possible number of soluble components. These are substrates and metabolic products, which diffuse and react in the biofilm within individual microbial cells. The cells grow, divide, and produce extracellular polymeric substances (EPS) in a multispecies model setting. The EPS matrix is described by a continuum representation as incompressible viscous fluid, which can expand and retract due to generation and consumption processes. The cells move due to a pushing mechanism between cells in colonies and by an advective mechanism supported by the EPS dynamics. Detachment of both cells and EPS follows a continuum approach, whereas cells attach in discrete events. Two case studies are presented for model illustration. Biofilm consolidation is explained by shrinking due to EPS and cell degradation processes. This mechanism describes formation of a denser layer of cells in the biofilm depth and occurrence of an irregularly shaped biofilm surface under nutrient limiting conditions. Micro-colony formation is investigated by growth of autotrophic microbial colonies in an EPS matrix produced by heterotrophic cells. Size and shape of colonies of ammonia and nitrite-oxidizing bacteria (NOB) are comparatively studied in a standard biofilm and in biofilms aerated from a membrane side.

Keywords: biofilm; mathematical model; discrete; individual; continuum; EPS; consolidation; nitrification; colony

INTRODUCTION

From the mid 1990s, new mathematical models have been developed to provide mechanistic representations for the factors controlling formation of complex 3-d biofilm morphologies (Wanner et al., 2005). Features included in this new generation of mathematical models are usually motivated by biofilm observations made with powerful new experimental tools such as the confocal laser scanning microscopy (CLSM, Neu and Lawrence, 1997), magnetic resonance imaging (MRI, Manz et al., 2003), or microsensors (De Beer et al., 1994).

Up to now, the 2-d and 3-d biofilm models could be divided in two general classes according to the way chosen for biomass representation: (i) discrete individual units or particles or (ii) a continuum body. Discrete particle models such as the cellular automata (CA, Picioreanu et al., 1998) or the individual-based models (IbM, Kreft et al., 2001), have been first developed and are now becoming widely applied to study effects of spatially multidimensional (2-d and 3-d) gradients in biofilms (see reviews in Picioreanu and Van Loosdrecht, 2003; Wanner et al., 2005). The benefit of using a particle-based model is that interactions at a local level may be modeled, that is, at the level of an individual bacterium. Particle-based models have been used for studies of the interaction between different species in a multidimensional biofilm setting (Kreft et al., 2001, 2004; Picioreanu et al., 2004). New local rules are easily added to describe more processes, such as detachment and attachment (Xavier et al., 2005b), structured biomass (Xavier et al., 2005a), and EPS (Kreft and Wimpenny, 2001; Xavier et al., 2005a). Using such local rules appeal to biologists because the rules can be motivated purely from biological principles, instead of analysis from a mathematical and physical framework. However, from a mathematical point of view, there are some drawbacks to the discrete models: (i) their output may depend on the sequence of execution of methods on the discrete objects and may introduce stochastic effects into the solutions, (ii) error analyses for discrete models are nontrivial; (iii) without a mathematical framework, from both an

Correspondence to: C. Picioreanu
Contract grant sponsor: KK foundation

analytic and a computational point of view, there is a risk that these models become more aesthetically driven than physically motivated (Eberl et al., 2001).

Continuum models, on the other hand, assume that the local variation within the biofilm matrix is averaged into a continuum body. Concepts such as the representative volume element (Wanner and Gujer, 1986) and methods like volume averaging (Wood and Whitacker, 1999) are used instead of the individual cell representation. Therefore, shapes, sizes, and, in general, local interactions between individual organisms are not directly taken into account in continuum biofilm models. These types of models are based upon explicit governing equations for conservation of mass and momentum, like in other mathematically more mature sciences. As a main advantage, a continuum biofilm description allows for the full use of the powerful framework of partial differential equations. This makes the computational process, that is, simulation, a matter of solving equations governed by a framework of numerical analysis, which is well developed in the area of computational physics. However, formulation and derivation of continuum models require a comprehensive mathematical skill and the computational algorithms are sometimes not trivial. Moreover, models of this type still lack the capability for studies of microbial ecology, since there is at present no multi-dimensional multi-species continuum model including a robust numerical framework. Successful models allowing the study of multiple conversions between different substrates and different types of bacteria are often based on the 1-d continuum model first introduced by Wanner and Gujer (1986). Multidimensional continuum models often describe a biofilm system consisting of a single species, such as the diffusion model by Eberl et al. (2001) or the viscous fluid model by Dockery and Klapper (2001). Adding additional species seems non-trivial, at least when it comes to the numerical implementation. Nevertheless, the first steps towards the derivation and implementation of a 3-d multi-species continuum biofilm model have been already made in Alpkvist (2005).

We believe that the continuum and discrete modeling approaches both have advantages and disadvantages. Therefore, in this study we propose a hybrid model, combining these two approaches. Experimental studies of material properties of a biofilms such as mechanical stress induced by fluid flow (Stoodley et al., 1999) suggest that the biofilm should be described as a viscous fluid (Klapper et al., 2002). Hence, using a viscous fluid continuum model for the biofilm matrix (made by extracellular polymeric substances, EPS) seems to be well justified. In this study, we explore the possibility of describing the biofilm by a continuum field on a global level and the interactions between individual bacteria in a discrete way using the IbM approach. The EPS will thus be modeled by a scalar field and not in a discrete IbM manner as by Kreft and Wimpenny (2001) or Xavier et al. (2005a). The benefits of this approach are: (1) a continuum viscous fluid description is well justified for the EPS field both by experimental facts and on physical grounds; (2) a continuum description of the biofilm at a global level will allow for a strict mathematical analysis and treatment of the model; (3) biofilm contraction is possible when some processes lead to loss of biofilm volume; (4) local interactions between different microbial species may be easily described and studied using the IbM approach; (5) individual variation of microbial cells may be taken into account.

In this article, we first present the governing framework of the model. Both the continuum and the discrete model components are here described in detail. Next, we present the computational steps needed to provide the simulation results. Finally, two case studies will illustrate the flexibility of this new approach. The case studies demonstrate the model capability to describe and explain biofilm phenomena otherwise very difficult to judge by other approaches, namely: (i) the biofilm consolidation (Laspidou and Rittmann, 2004) and (ii) growth of colonies embedded in an EPS matrix.

MODEL DESCRIPTION

It is convenient to organize the construction of a mathematical biofilm model based on several conceptual criteria: (1) the space division into different computational *domains*; (2) the nature and behavior of the relevant *components*; and (3) the *processes* taken into account for each class of components (Wanner et al., 2005). All processes affecting each component in each domain are mathematically linked together into balance equations.

Spatial Domains and Geometry

Modeling the whole system with the same set of equations is very inefficient due to the various spatial and temporal scales at which processes occur and components exist. Therefore, the biofilm system is typically divided into various sub-domains (compartments). For each sub-domain, simplifying assumptions about the components and processes are made, along with decisions regarding the spatial and temporal resolutions needed (Wanner et al., 2005).

The spatial sub-domains defined for this model are the biofilm itself Ω_F, the bulk liquid Ω_B, and a mass transfer boundary layer Ω_L (MTBL) (Fig. 1). In principle, the biofilm system can be modeled developing on any substratum geometry (see Picioreanu et al., 1999, 2001). A planar surface of dimensions L_X and L_Y is chosen here as an example. The substratum forms the system boundary Γ_S at $z=0$, whereas the system size in the direction normal to substratum is L_Z. A MTBL through which the soluble components diffuse between the bulk liquid and the solid biofilm exists on top of the biofilm. Because the focus of this study is in the buildup of a better model for the biofilm phase, the shape of the top limit of the MTBL, Γ_{BL}, is just chosen to follow the geometry of the biofilm surface at a certain distance. The MTBL is created by a dilation algorithm originating on the biofilm surface Γ_{LF} (Glasbey and Horgan, 1994). The MTBL thickness, L_L, is therefore defined as the largest thickness of this layer above the biofilm surface

DOI 10.1002/bit

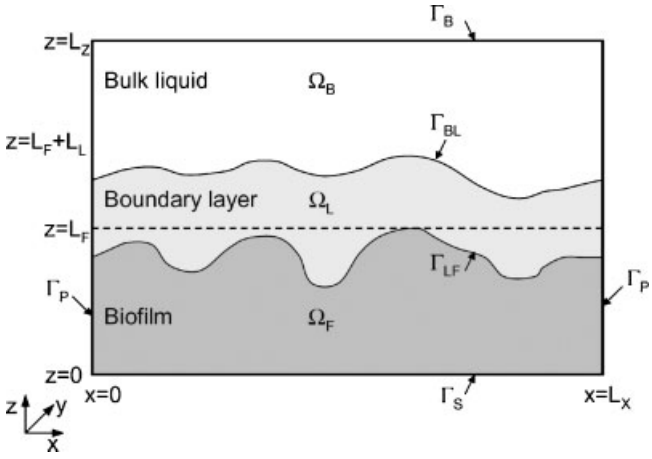

Figure 1. Geometry and sub-domains of the model biofilm system.

(Fig. 1). Other approaches are possible with implications discussed in Picioreanu et al. (2000a). The interface between MTBL and the bulk liquid on top of it is time dependent and situated at a distance L_L from the tallest biofilm feature at the current time.

Components

The common practice in biofilm modeling is to divide components into dissolved and particulate. Dissolved components are soluble chemical species, including diverse substrates, metabolic intermediates, and various products of microbial conversion processes (e.g., organic compounds, O_2, NH_3, NO_3^-). Particulate components are the materials that form the biofilm solid phase, such as microbial cells, inert material, and the EPS. The particulates are physically attached to each other or to the substratum.

The distinction between particulate and dissolved components has been generated by the difference in size of the unit components of each class: the molecules of dissolved components are much smaller than the microbial cells forming the main type of particulate components. This very important difference has several significant effects. First, transport processes in the biofilm are different, that is, particulate components do not diffuse, while soluble components do. Secondly, the characteristic times of the processes related to the two types of components are notably different: processes associated with the particulate components are much slower than those are for the dissolved components. Model simulations can be made computationally more efficient by separating the processes associated with the dissolved and particulate components.

Dissolved Components

There are n_S dissolved components i represented by continuum fields of concentration S_i for component i. Soluble chemical components exist in all model domains.

Particulate Components

The present model introduces a further differentiation among the particulate components. On one hand, microbial cells are regarded as discrete entities, and they are in general treated according to the individual-based methodology established by Kreft et al. (1998, 2001) and Picioreanu et al. (2004). On the other hand, the biofilm matrix formed by EPS is considered a continuum. Therefore, the development of the biofilm as a whole will be governed by the behavior and interactions between discrete and continuum entities. In the current model, the particulate components exist only in the biofilm domain.

Discrete Microbial Cells

The 3-d biofilm structure contains a set of n_P discrete non-overlapping hard spheres of biomass called biomass particles. These particles can represent the discrete microbial cells. Each biomass particle P is characterized by a position vector (x, y, z), a radius R_P, and a vector of biomass composition $m_{X,i,P}$. It is assumed that the biofilm consists of n_X types of biomass (numbered $i = 1, 2, \ldots, n_X$). The separation of active biomass into different categories is usually based on differences in metabolism. Each biomass particle P may therefore contain one type of active biomass and different fractions of other biomass components (e.g., inert biomass, storage polymers, etc.) (Xavier et al., 2005a). The total mass $m_{X,P}$ of the particle P is, therefore, the sum of all biomass components, $m_{X,i,P}$. It is assumed that the density of the biomass type i in a biomass particle is $\rho_{X,i}$. When the biomass of the particle changes in time, volume and radius change accordingly. In the 2-d model, the biomass particles are cylinders with length h spanning the whole domain:

$$R_P = \left(\frac{3}{4\pi} \sum_{i=1}^{n_X} \frac{m_{X,i,P}}{\rho_{X,i}} \right)^{\frac{1}{3}} \text{in 3-d},$$
$$R_P = \left(\frac{1}{4\pi h} \sum_{i=1}^{n_X} \frac{m_{X,i,P}}{\rho_{X,i}} \right)^{\frac{1}{2}} \text{in 2-d} \quad (1)$$

Continuum EPS

In this novel model, the biofilm matrix containing EPS is treated as a continuum field, which embeds the discrete microbial cells. The EPS behavior is described as an incompressible viscous fluid moving according to Darcy's law (see next section).

Processes and Balance Equations

Three universal types of processes take place in biofilm systems. *Transformations*, also called conversions or reactions, describe the production or consumption of a dissolved or particulate component. *Transport* processes describe the

motion of mass within a domain, whereas *transfer* processes describe the exchange of mass between different domains. For any component, a general mass balance can be set up as the partial differential equation:

$$\frac{\partial C}{\partial t} = -\left(\frac{\partial j_x}{\partial x}+\frac{\partial j_y}{\partial y}+\frac{\partial j_z}{\partial z}\right) + r \qquad (2)$$

where t is time, x, y, and z are spatial coordinates, C is the component concentration, $\mathbf{j}=(j_x, j_y, j_z)^{\mathrm{T}}$ is the mass flux vector and r is the net production rate of the component. The inter-domains transfer processes will be taken into account by the boundary conditions associated with Equation (2). The tasks of setting specific mathematical expressions for $\mathbf{j}$ and r, depending on the processes that are significant for the component and domain considered, will be discussed in the following sub-sections.

Dissolved Components

Dissolved components can be produced or consumed in several biotic or abiotic *transformation* processes. It is assumed here that all substrate *transport* takes place only by molecular diffusion. Conditions in which other mass transport mechanisms such as convection play a significant role were analyzed in other studies (Eberl et al., 2000; Picioreanu et al., 2000a; Wanner et al., 2005).

Substituting the molecular diffusion flux vector given by Fick's first law

$$\mathbf{j}_{\mathrm{S}} = -D\nabla S = \left(-D\frac{\partial S}{\partial x}, -D\frac{\partial S}{\partial y}, -D\frac{\partial S}{\partial z}\right)^{\mathrm{T}} \qquad (3)$$

in the general mass balance Equation (2), the non-steady state mass balance for any dissolved component i becomes

$$\frac{\partial S_i}{\partial t} = \frac{\partial}{\partial x}\left(D_i\frac{\partial S_i}{\partial x}\right)+\frac{\partial}{\partial y}\left(D_i\frac{\partial S_i}{\partial y}\right)+\frac{\partial}{\partial z}\left(D_i\frac{\partial S_i}{\partial z}\right)+r_{S,i} \qquad (4)$$

where S_i is the concentration of the dissolved component. Note that in Equation (4) the diffusion coefficient D_i can be variable in space ($D_i = D_i(\mathbf{x})$), accounting for different diffusivities in the various places in the biofilm and in the surrounding liquid. The net reaction rate $r_{S,i}$ is the algebraic sum of the rates of all individual processes that produce or consume that specific soluble component. In a general case, the mass balance (Eq. (4)) would apply for all dissolved components in all computational sub-domains. However, particular simplified forms are used here for different sub-domains. In MTBL sub-domain Ω_{L}, the reaction term $r_{S,i}$ is assumed to be zero for all dissolved components. In the bulk liquid sub-domain Ω_{B} the assumption of complete mixing is accomplished by having a very large diffusion coefficient, $D_i \to \infty$. For simplicity, no transformations can occur in the bulk liquid sub-domain.

The boundary conditions needed to solve the mass balance Equation (4) reflect the particular setting of the modeled biofilm system. In order to simplify the analysis of model results, the whole bulk liquid domain is made an infinite reservoir supplying nutrients in concentrations $S_i = S_{\mathrm{B},i}$. At $z = L_Z$ (top of the computational domain Γ_{B}) constant concentration of all soluble components is assumed. The substratum on which the biofilm develops (at $z=0$) is assumed impermeable (if not otherwise stated), so that a no-flux condition can be applied on Γ_{S}. To minimize unwanted small-scale effects, the lateral system boundaries (Γ_{P}) were connected and formed a so-called "periodic" or "cyclic" boundary type (see also Picioreanu et al., 1998, 2004). The bulk/boundary layer (Γ_{BL}) and the boundary layer/biofilm (Γ_{LF}) interfaces are considered as internal boundaries where concentration continuity conditions apply. For the initial state at $t=0$, a uniform distribution of concentrations throughout the whole domain was assumed, with $S_i = S_{\mathrm{B},i}$.

Because the diffusion and reaction of dissolved components are very fast compared with the rates of biological processes (e.g., microbial growth rates), we may consider a quasi-steady state for the balance Equation (4) each time when the particulate component dynamics is solved. Hence, the solved equation for each soluble component in the system ($i = 1,\ldots,n_{\mathrm{S}}$) is:

$$\begin{cases} -\nabla\cdot(D_i\nabla S_i) = r_{\mathrm{S},i} & \text{in } \Omega \text{ with } D_i \to \infty \text{ in } \Omega_{\mathrm{B}} \\ & \text{and } , r_{\mathrm{S},i} = 0 \text{ in } \Omega_{\mathrm{B}}\cup\Omega_{\mathrm{L}} \\ \dfrac{\partial S_i}{\partial z} = 0 & \text{on } \Gamma_{\mathrm{S}} \\ S_i = S_{\mathrm{B},i} & \text{on } \Gamma_{\mathrm{B}} \end{cases} \qquad (5)$$

Particulate Components

Similarly with the dissolved components, the particulate components (e.g., cells and EPS) within the biofilm undergo transformation and transport processes. Therefore, the biomass follows the same basic conservation principle expressed by Equation (2).

Global Advective Transport Process

Production of particulate components will generate biofilm volume, whereas consumption will decrease its volume. One can imagine that growing biomass will generate a sort of internal pressure in the biofilm, which we will call "biomass pressure." Therefore, the *transport* of particulates in a growing biofilm can be seen as the movement away from the areas with high pressure. We may assume that this movement can be described by an advection process and the advective flux of biomass is given by

$$\mathbf{j}_X = X\mathbf{u} = (Xu_x, Xu_y, Xu_z)^{\mathrm{T}} \qquad (6)$$

where X is the concentration of biomass (cells or EPS) in the biofilm. The flow field supporting biomass advection is described by the advective velocity vector $\mathbf{u}=(u_x, u_y, u_z)^{\mathrm{T}}$. Because one wants biomass transport dependent on the "biomass pressure," the overall transport of biomass within

DOI 10.1002/bit

the biofilm region is assumed to follow the fluid dynamics constitutive relation known as Darcy's law:

$$u = -\lambda \nabla p \tag{7}$$

where $\lambda = \lambda(\mathbf{x})$ is the Darcy parameter, a material property inversely proportional with the dynamic viscosity η of the medium, and $p = p(\mathbf{x})$ is the pressure generated by the growing or shrinking biofilm. The linear Darcy law holds for flows at low Reynolds numbers, when driving forces are small and balanced only by the viscous forces. Using the Darcy law as a model for biomass flow within the biofilm was introduced and analyzed in Dockery and Klapper (2001). The biomass in the system consists of both bacterial mass and EPS with a composition that may vary in space. Different viscosities can be assigned to different biomass types and EPS, thus affecting the biofilm flow field both locally and globally.

Based on Equation (6), the advective flux of each particulate component i will be written as:

$$\mathbf{j}_{X,i} = \varepsilon_i \rho_{X,i} \mathbf{u} \tag{8}$$

given the volume fraction ε_i of that component in the biofilm, and $\rho_{X,i}$ the density of a particulate phase (i.e., any cell type or EPS). If one separates the EPS phase from the microbial cell phase, one can write the total biofilm volume composition as:

$$\sum_{i=1}^{n_X} \varepsilon_i + \varepsilon_{\mathrm{E}} = \varepsilon_{\mathrm{C}} + \varepsilon_{\mathrm{E}} = 1 \tag{9}$$

The mass balances for all biomass types and for EPS can therefore be obtained by substituting the fluxes (Equation. (8)) into the general mass balance Equation (2). One obtains Equation (10) as mass balance for the microbial cells and Equation (11) for the EPS:

$$\frac{\partial(\varepsilon_i \rho_{X,i})}{\partial t} = -\nabla \cdot (\varepsilon_i \rho_{X,i} \mathbf{u}) + r_{X,i} \quad \text{for all } i = 1, 2, \ldots n_X \tag{10}$$

$$\frac{\partial(\varepsilon_{\mathrm{E}} \rho_{X,\mathrm{E}})}{\partial t} = -\nabla \cdot (\varepsilon_{\mathrm{E}} \rho_{X,\mathrm{E}} \mathbf{u}) + r_{X,\mathrm{E}} \tag{11}$$

The biomass *transformation* rates $r_{X,i}$ and $r_{X,\mathrm{E}}$ express the net production of microbial cells and EPS, respectively. They are coupled to the solute rates $r_{\mathrm{S},i}$ by stoichiometric coefficients.

By summation of Equations (10) and (11) for all microbial species and EPS, and using Equation (9) with the assumption of constant densities of particulate phases in space and time, one obtains:

$$0 = -\nabla \cdot \mathbf{u} + \sum_{i=1}^{n_X} \frac{r_{X,i}}{\rho_{X,i}} + \frac{r_{X,\mathrm{E}}}{\rho_{X,\mathrm{E}}} \tag{12}$$

Finally, substitution of Darcy's relationship (7) into Equation (12) gives the law governing the biomass pressure:

$$-\nabla \cdot (\lambda \nabla p) = \sum_{i=1}^{n_X} \frac{r_{X,i}}{\rho_{X,i}} + \frac{r_{X,\mathrm{E}}}{\rho_{X,\mathrm{E}}} \tag{13}$$

This second order elliptic partial differential equation simply states that, in the case of a growing biofilm, the pressure generated by local biomass production is released by expanding the biofilm volume. Similarly, in places where cells or EPS decay, the depression will lead to a shrinking biofilm.

The liquid phase outside the biofilm has a very small viscosity compared to an obviously much higher viscosity of the biofilm biomass. Consequently, because only small perturbations in pressure field are needed to induce movement in the liquid surrounding the biofilm, it is reasonable to consider the pressure in the liquid domains Ω_{L} and Ω_{B} to be constant compared to the pressure within the biofilm domain Ω_{F}. Therefore, we may impose a zero pressure in the liquid domains, and a zero gradient of pressure normal on the biofilm surface on the biofilm side.

This derivation let us arrive at the following system of equations for the pressure that governs the global flow field in the biofilm:

$$\begin{cases} -\nabla \cdot (\lambda \nabla p) = R_X & \text{in } \Omega_{\mathrm{F}} \\ \frac{\partial p}{\partial \mathbf{n}} = 0 & \text{on } \Gamma_{\mathrm{LF}} \\ p = 0 & \text{in } \Omega_{\mathrm{L}} \cup \Omega_{\mathrm{B}} \end{cases} \tag{14}$$

where R_X is a global rate of biofilm volume generation, deriving from Equation (13). $\mathbf{n}$ is the direction normal on the biofilm interface. Using the gradient of the pressure field calculated from Equation (14), it is possible to compute from Equation (7) the advection velocity $\mathbf{u}$ of the biomass flow.

Interface Movement and Detachment Process

The biofilm advection velocity field $\mathbf{u}$ will move the biofilm interface accordingly. Imagining a point x on the biofilm interface Γ_{LF} following the interface during biofilm expansion or shrinking, this point will have the interface speed in the normal direction on the interface given by

$$\frac{\mathrm{d}x}{\mathrm{d}t} = \mathbf{n} \cdot \mathbf{u} - u_{\mathrm{det}} \tag{15}$$

where $\mathbf{n}$ is the normal of the biofilm interface and u_{det} is the biofilm detachment velocity. Substituting the flow field velocity we may write

$$\frac{\mathrm{d}x}{\mathrm{d}t} = -\mathbf{n} \cdot \lambda \nabla p - u_{\mathrm{det}}(x, \rho_{X,i}, \rho_{X,E}, \tau_w, \ldots) \tag{16}$$

The detachment velocity can be any function of, for example, biofilm surface position, biofilm composition in cells and EPS, liquid shear τ_w, etc. (see Xavier et al., 2005b). A detachment velocity function proportional with the square

of the distance from substratum is used here:

$$u_{\mathrm{det}} = k_{\mathrm{det}} z^2 \tag{17}$$

After the biofilm interface has been moved in a given time step (Eq. (16)), the discrete cells that may exist outside the biofilm sub-domain Ω_F are simply removed from the system.

Processes of Growth and Division of Individual Cells

The growth of each biomass type i with time is described by an ordinary differential equation representing the mass balance for each biomass particle P:

$$\frac{\mathrm{d}m_{X,i,P}}{\mathrm{d}t} = r_{X,i} \qquad \begin{array}{l}\text{for each } P = 1, 2, \ldots, n_P \\ \text{and each } i = 0, 1, \ldots, n_X\end{array} \tag{18}$$

The net reaction rates for generation of active biomass $r_{X,i}$ are typically functions of the active biomass of the particle, $m_{X,i,P}$, and concentrations S_i of various soluble components present at the center (x, y, z) of the biomass sphere. An initial distribution of biomass particles at time $t = 0$ must be defined. It is assumed that all $n_{X,i,0}$ initial biomass particles have mass m_0 and radius $R_{P,0}$. They are randomly distributed on the planar substratum surface at $(x, y, R_{P,0})$.

If sufficient nutrients exist in the environment, the bacterial mass contained in each particle will grow according to Equation (18). However, the total biomass in a spherical biomass particle is assumed limited to a maximum value, $\Sigma_i m_{X,i,P} < m_{X,\max}$, that is independent of growth rate for the sake of simplicity (Kreft et al., 2001; Picioreanu et al., 2004). When this maximum biomass in a sphere is reached, a new ''daughter'' sphere is created, touching the ''mother'' sphere in a randomly chosen direction. Part of the biomass contained in the ''mother'' is then redistributed to the ''daughter'' sphere. In order to break possible colony-synchronized divisions occurring when one particle is split in precisely equal parts (Kreft et al., 2001), between 40 and 60% of the biomass in the ''mother'' particle is redistributed (percentage chosen with a uniform distribution).

Transport of Cells

An important point is that Equation (10) is not explicitly solved, but instead, an IbM framework for modeling shoving of individual cells is invoked. This assumption is justified by three arguments. First, bacteria are discrete entities, thus a discrete representation is physically more natural. Second, it has been numerically shown (Picioreanu et al., 2004) that the IbM framework for cell transport describes its continuum counterpart at least in a 1-d case. Third, a simple mechanical analog exists with hard spheres connected by repulsive linear springs.

The transport of individual microbial cells within the biofilm is assumed to occur due to two distinct mechanisms: global advection and individual shoving. The two mechanisms are schematically depicted in Figure 2. First, the microbial cells within the biofilm stick to the EPS network. Biofilm volume production (as well as volume loss) will introduce forces that travel through the EPS network and in turn create pressure gradients (described in section ''Global advective transport''). The build up of pressure will produce a flow field that moves both the cells and EPS. We assume this flow field to be well approximated by the Darcy law (Eq. 7) on a global level. Second, we introduce small local deviations in the flow field, variable on the individual bacterium level. This individual variation within the flow field is governed by the cell shoving method characteristic to the IbM described in Kreft et al. (2001) and Picioreanu et al. (2004). The cells are treated as hard bodies in the model, which are not allowed to overlap. Individual cells (biomass spheres) are therefore shoved when they get too close to each other.

On the global scale, we assume these local variations due to shoving to average out. This leads us to introduce a restriction on the flow field of cells. Practically, we restrict the local shoving flow field to differ from the global Darcy flow only in directions perpendicular to the global flow field. Thus, we write the composite advective velocity for a cell, $\mathbf{u}_{\mathrm{cell}}$:

$$\mathbf{u}_{\mathrm{cell}} = \mathbf{u}_{\mathrm{shov}} + \left(1 - \frac{\langle \mathbf{u}, \mathbf{u}_{\mathrm{shov}} \rangle}{||\mathbf{u}||}\right)\mathbf{u} \tag{19}$$

where $\mathbf{u}$ is global Darcy velocity given by Equation (7) and $\mathbf{u}_{\mathrm{shov}}$ the velocity from the shoving interaction of hard-spheres, given by mechanisms described in Picioreanu et al. (2004).

Attachment of Individual Cells

Besides detachment of cells and EPS, attachment of individual cells from the liquid domain to the biofilm surface is also considered in the present model. A number of biomass

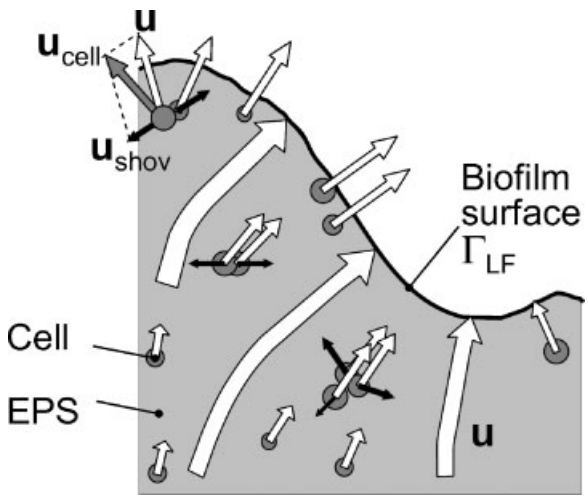

Figure 2. Movement of EPS in the biofilm is governed by a global advection speed $\mathbf{u}$. Cells move by a velocity $\mathbf{u}_{\mathrm{cell}}$, which is the resultant of the global advection flow $\mathbf{u}$ and a local shoving velocity $\mathbf{u}_{\mathrm{shov}}$.

DOI 10.1002/bit

particles (i.e., cells) may be added in each time step in the biofilm sub-domain Ω_F, at a position adjacent to the biofilm surface Γ_{LF}. In this study, a fraction f_{ata} of the detached cells in a time interval will be re-attached at each time step. The attachment process will happen at random places next to the biofilm surface. Cell attachment is important in biofilm systems where minor microbial species (e.g., slow-growing organisms) must be continuously supplied to the biofilm (see model case studies, Example 2).

MODEL SOLUTION

The continuum fields describing physical quantities such as soluble and particulate component concentrations (S_i and X_i, respectively), and biomass pressure p, are discretized and associated with a uniform computational space with mesh size h. Time advances in non-uniform increments, with time step of size τ_n at iteration n.

The dynamics of soluble components due to transport and reaction is very fast (e.g., in the order of seconds) compared with the dynamics of particulate components (e.g., in the order of hours to days). Following time-scale arguments, the solution of biomass balances can be decoupled from that of substrate diffusion-reaction mass balances (Picioreanu et al., 2000b). Due to this time separation assumption, the algorithm for different model processes can be executed sequentially. The different steps in the numerical approximation algorithm are described by the pseudo-code in Figure 3.

I. Initialization

- time $t_n \leftarrow 0$
- sub-domains Ω_F, Ω_L and Ω_B
- initial substrate concentrations $S_i(t_n,\mathbf{x}) \leftarrow S_i(0,\mathbf{x})$, initial EPS distribution $X_E(t_n,\mathbf{x}) \leftarrow X_E(0,\mathbf{x})$
- initial microbial cells distribution $m_{X,i,P}(t_n,\mathbf{x},R_P) \leftarrow m_{X,i,P}(0,\mathbf{x}_0,R_{P,0})$ and $X_i(t_n,\mathbf{x}) \leftarrow X_i(0,\mathbf{x})$

II. Time-stepping

do

A. Dynamics of EPS particulate components and biofilm volume

1- Biomass pressure distribution

Solve biomass pressure $p(t_n,\mathbf{x})$ from Eq. (14).

[$S_i(t_n,\mathbf{x})$, $X_i(t_n,\mathbf{x})$, $X_E(t_n,\mathbf{x})$ used to calculate the source term of volume change due to microbial processes]

2 - Advective velocity distribution

Calculate advective flow velocity $\mathbf{u}(t_n,\mathbf{x})$ from Eq. (7).

[$p(t_n,\mathbf{x})$ is used. The maximum time step from CFL condition is $\tau_n < h/\max_{\Omega_F}|\mathbf{u}|$].

3 - Volume change

Move the biofilm interface $\Gamma_{LF}(t_n)$ by Eq. (16).

[$\mathbf{u}(t_n,\mathbf{x})$ and a detachment function u_{det} are used. The sub-domains size and shape are changed]

B. Dynamics of microbial cell particulate components

4 - Cells detachment

Remove cells falling outside of the new biofilm sub-domain Ω_F.

[Level set $\phi(t_n,\mathbf{x})$ is used to track biofilm surface and removal of biomass "islands" disconnected from substratum is performed]

5 - Cells mass change (growth and decay)

Change mass of cells $m_{X,i,P}$ by Eq. (18).

[$S_i(t_n,\mathbf{x})$, $X_i(t_n,\mathbf{x})$ and $X_E(t_n,\mathbf{x})$ are used to calculate the process rates]

6 - Cells division

Split mass of cells when $m_{X,i,P} > m_{X,i,max}$.

7 - Cells attachment

Add new cells on the biofilm surface.

8 - Cells transport

Move cells by IbM shoving mechanism combined with global advection.

[$\mathbf{u}(t_n,\mathbf{x})$ is used]

C. Dynamics of dissolved components

9 - Reaction-diffusion mass balances

Solve for soluble component concentrations $S_i(t_n,\mathbf{x})$ the equation system (5).

[$S_i(t_n,\mathbf{x})$, $X_i(t_n,\mathbf{x})$ and $X_E(t_n,\mathbf{x})$ are used to calculate the process rates]

D. Time advancement

$t_n \leftarrow t_n + \tau_n$

while $t_n < t_N$

Figure 3. Algorithm steps used for solution of the biofilm model.

There are n_S+1 second order elliptic partial differential equations in the model, describing the spatial dynamics of soluble components and of biomass pressure (steps 1 and 9). A very efficient solution to this problem is the multigrid method introduced by Brandt (1977). The full approximation storage (FAS) multigrid algorithm for non-linear elliptic systems solves a problem scaling only linearly in computational time for the number of unknowns. The algorithm used here is derived from Press et al. (1997) and its use in a biofilm model was described in Picioreanu et al. (2004) and Xavier et al. (2005a).

Solving for biofilm volume increment puts constraints upon the time step. The Courant–Friedrich-Lévy (CLF) condition restricts the spatial flow of information to the maximum of one grid cell for each time step, ensuring stable time stepping. To describe the time-evolution of the biofilm, we apply the numerical framework provided by the level-set method (Sethian, 1996, 1999). A function $\phi = \phi(t, \mathbf{x})$ is constructed to be the signed distance of $\mathbf{x}$ from the interface Γ_{LF}. In particular, we have $\phi(t, \mathbf{x}) = 0$ for $\mathbf{x}$ on Γ_{LF} and let the biofilm subset of Ω_F be the negative set by imposing $\phi(t, \mathbf{x}) < 0$ there. Encoding the motion of Γ_{LF} we take the motion of a point $\mathbf{x} = \mathbf{x}(t)$ on the interface Γ_{LF} by

$$\phi(t, \mathbf{x}) = 0, \quad \text{for any time } t \tag{20}$$

Differentiating with respect to time, we may write the level-set equation of motion:

$$0 = \nabla\phi(t, \mathbf{x}(t)) \cdot \mathbf{x}'(t) + \frac{\partial\phi}{\partial t}(t, \mathbf{x}(t)) \tag{21}$$

where $\mathbf{x}'(t)$ is the speed of the interface governed by the Darcy flow condition (7). The level-set equation of motion (21) is solved using an Euler integration step in time, employing a third order weighted essentially non-oscillatory (WENO) scheme for the spatial discretization of derivatives of $\phi(t, \mathbf{x}(t))$ (Jiang and Peng, 2000).

The transport of cells may be divided into a two-step algorithm. First, the discrete transport mechanism (shoving) of the IbM framework is applied. This allows an individual variation in the transport for each cell at a local level. At the end of this phase the distance $\mathbf{x}_{shov}$ a cell has been transported by the discrete shoving algorithm is calculated. Using the time step τ_n and this advected distance, the local flow field $\mathbf{u}_{shov}$ is calculated. We assume transport of each cell along the trajectory of the global flow field $\mathbf{u}$ to be unperturbed by the local $\mathbf{u}_{shov}$. In the second phase, a projection step of the local flow field $\mathbf{u}_{shov}$ on the global field $\mathbf{u}$ is performed. Cells are moved with a speed corresponding to the second term in Equation (19).

MODEL CASE STUDIES

The model introduced here is a general framework that can be used to describe various biofilm systems, with any number of soluble components and any number of particulate species in 2-d or 3-d spaces. Therefore, a model user will have to make a selection of relevant components and processes when building the model. This section will present a series of two model applications illustrating biofilm phenomena that are difficult or even impossible to be described by previously published model approaches.

Case 1: Biofilm Consolidation

Transformation of one particulate biomass component into another is a common concept in biofilm modeling, that is, biomass decay from active to inert biomass, or EPS production and degradation. If the particulate components involved in the process have different densities, the biomass transformation process will change the biofilm volume. This volume change can either be an expansion, for example, in the case of light-density EPS production or shrinking, for example, when the EPS matrix is degraded. Using this hybrid-model approach, the global biomass flow in the biofilm is governed by pressure gradients generated by such potential volumetric changes. Accordingly, volume decrease in the depth of the biofilm (e.g., due to a net EPS loss) will in turn produce a pressure gradient allowing biomass to be transferred into this region. This shrinking process will create a gradient in the spatial biomass density distribution, phenomenon that may be called "consolidation," as suggested by Bishop et al. (1995) and Laspidou and Rittmann (2004).

To test the consolidation hypothesis, the hybrid model was applied to a simple biofilm system previously simulated by the IbM approach (Xavier et al., 2005b). Stoichiometry and process kinetics of this system in two simulated cases are presented in Table I. Model parameters are given in Table II. First, a 2-d simulation of homogeneous biofilm formation at a relatively high oxygen concentration (4 g/m^3) and non-limiting COD concentration (100 g/m^3) is presented in Figure 4 (case *1A2d*). By introducing a detachment function proportional to the square of the biofilm height, a quasi-steady-state in biofilm thickness can be achieved. This quasi-steady-state in biofilm thickness has been many times reported in the operation of biofilm reactors over extended periods of time (e.g., in biofilm airlift reactors, see Kwok et al., 1998). Keeping the biofilm thickness fairly stable in time facilitates investigation of development of biofilm density gradients over extended time periods, thus for rather old biofilms, as seen in Figure 4. While the biofilm thickness is reaching a steady-state, the number of cells in the biofilm is still constantly increasing (Fig. 5). As the density of the cell phase is assumed higher than the density of the EPS phase, the overall biofilm density is increasing in time. A second 2-d simulation of heterogeneous biofilm development at relatively lower oxygen and COD concentrations (1.5 gO_2/m^3 and 1.5 gCOD/m^3) is presented in Figure 6 (case *1B2d*). Finally, to illustrate the generality of this approach, two 3-d simulations of homogeneous (case *1A3d*) and heterogeneous (case *1B3d*) biofilm formation are shown in Figure 7.

DOI 10.1002/bit

Table I. Stoichiometry matrix and kinetics for the biological processes modeled.

	Soluble components					Particulate components				
Process	Substrate S_S (gCOD/m^3)	Oxygen S_{O_2} (gO_2/m^3)	Ammonia S_{NH_3} (gN/m^3)	Nitrite S_{NO_2} (gN/m^3)	Nitrate S_{NO_3} (gN/m^3)	Heterotrophs X_H (gCOD/m^3)	AOB X_{AOB} (gCOD/m^3)	NOB X_{NOB} (gCOD/m^3)	Inerts X_I (gCOD/m^3)	EPS X_E (gCOD/m^3)
1. Substrate uptake by aerobic heterotrophs	-1	$-(1-Y_H-Y_E)$				Y_H				Y_E
2. Decay heterotrophs	$1-Y_I$					-1			Y_I	
3. EPS decay	1									-1
4. Nitrite uptake by denitrifying heterotrophs	-1			$-\frac{1-Y_H-Y_E}{1.71}$		Y_H				Y_E
5. Nitrate uptake by denitrifying heterotrophs	-1				$-\frac{1-Y_H-Y_E}{2.86}$	Y_H				Y_E
6. Growth of ammonia-oxidizing bacteria (AOB)		$-\frac{3.42-Y_{AOB}}{Y_{AOB}}$	$-\frac{1}{Y_{AOB}}$	$\frac{1}{Y_{AOB}}$			1			
7. Growth of nitrite-oxidizing bacteria (NOB)		$-\frac{1.15-Y_{NOB}}{Y_{NOB}}$		$-\frac{1}{Y_{NOB}}$	$\frac{1}{Y_{NOB}}$			1		
8. Decay AOB	1-Y_I						-1		Y_I	
9. Decay NOB	1-Y_I							-1	Y_I	
Process			Rate							
1. Substrate uptake by aerobic heterotrophs			$q_{S,H,max}\cdot X_H\cdot\frac{S_S}{K_{S,H}+S_S}\cdot\frac{S_{O_2}}{K_{O_2,H}+S_{O_2}}$							
2. Decay heterotrophs			$b_H\cdot X_H$							
3. EPS decay			$b_E\cdot X_E$							
4. Nitrite uptake by denitrifying heterotrophs			$\eta_H\cdot q_{S,H,max}\cdot X_H\cdot\frac{S_S}{K_{S,H}+S_S}\cdot\frac{S_{NO_2}}{K_{NO_2,H}+S_{NO_2}}\cdot\frac{K_{O_2,H}}{K_{O_2,H}+S_{O_2}}$							
5. Nitrate uptake by denitrifying heterotrophs			$\eta_H\cdot q_{S,H,max}\cdot X_H\cdot\frac{S_S}{K_{S,H}+S_S}\cdot\frac{S_{NO_3}}{K_{NO_3,H}+S_{NO_3}}\cdot\frac{K_{O_2,H}}{K_{O_2,H}+S_{O_2}}$							
6. Growth of ammonia-oxidizing bacteria (AOB)			$\mu_{AOB,max}\cdot X_{AOB}\cdot\frac{S_{O_2}}{K_{O_2,AOB}+S_{O_2}}\cdot\frac{S_{NH_3}}{K_{NH_3,AOB}+S_{NH_3}}$							
7. Growth of nitrite-oxidizing bacteria (NOB)			$\mu_{NOB,max}\cdot X_{NOB}\cdot\frac{S_{O_2}}{K_{O_2,NOB}+S_{O_2}}\cdot\frac{S_{NO_2}}{K_{NO_2,NOB}+S_{NO_2}}$							
8. Decay AOB			$b_{AOB}\cdot X_{AOB}$							
9. Decay NOB			$b_{NOB}\cdot X_{NOB}$							

Processes 1–3 were the only processes active in Case 1, whereas all processes (1–9) were considered in Case 2. Empty table entries are effectively zero stoichiometric coefficients.

Table II. Model parameters.

Parameters	Description	Value						Units
		1A2d	1B2d	1A3d	1B3d	2A2d	2B2d	
Solute components								
S_{B,O_2}	Bulk concentration of oxygen	4	1.5	4	0.5	10	1	g_{O_2}/m^3
$S_{B,S}$	Bulk concentration of substrate	100	1.5	100	100	3	3	$g_{COD,S}/m^3$
S_{B,NH_3}	Bulk concentration of ammonia	—	—	—	—	10	10	g_N/m^3
S_{B,NO_2}	Bulk concentration of nitrite	—	—	—	—	0	0	g_N/m^3
S_{B,NO_3}	Bulk concentration of nitrate	—	—	—	—	0	0	g_N/m^3
Particulate components								
ρ_H	Density of heterotrophs	200000	200000	200000	200000	200000	200000	$g_{COD,X}/m^3$
ρ_I	Density of inert biomass	200000	200000	200000	200000	200000	200000	$g_{COD,X}/m^3$
ρ_E	Density of EPS	33000	33000	33000	33000	33000	33000	$g_{COD,X}/m^3$
ρ_{AOB}, ρ_{NOB}	Density of AOB and NOB	—	—	—	—	200000	200000	$g_{COD,X}/m^3$
$n_{X,H,0}$	Initial number of heterotrophic cells	250	250	500	500	200	200	
$n_{X,AOB,0}$	Initial number of AOB cells	—	—	—	—	20	20	
$n_{X,NOB,0}$	Initial number of NOB cells	—	—	—	—	20	20	
Reaction stoichiometry								
Y_H	Yield of heterotrophic biomass on substrate	0.206	0.206	0.206	0.206	0.206	0.206	$g_{COD,X}/(g_{COD,S})$
Y_E	Yield of EPS on substrate	0.289	0.289	0.289	0.289	0.289	0.289	$g_{COD,E}/(g_{COD,S})$
Y_I	Yield of inert biomass	0.4	0.4	0.4	0.4	0.4	0.4	$g_{COD,X}/(g_{COD,X})$
Y_{AOB}	Yield of AOB on N-ammonia	—	—	—	—	0.15	0.15	$g_{COD,X}/(g_N)$
Y_{NOB}	Yield of NOB on N-nitrite	—	—	—	—	0.041	0.041	$g_{COD,X}/(g_N)$
Reaction rate								
Heterotrophs (H)								
$q_{S,H,max}$	Maximum specific substrate uptake rate	22.85	22.85	22.85	22.85	22.85	22.85	$g_{COD,S}/g_{COD,X}/day$
b_H	Decay rate constant	0.079	0.079	0.079	0.079	0.079	0.079	1/day
b_E	EPS hydrolysis and decay rate constant	0.336	0.336	0.336	0.336	0.336	0.336	1/day
$K_{S,H}$	Substrate saturation constant	4.0	4.0	4.0	4.0	4.0	4.0	$g_{COD,S}/m^3$
$K_{O,H}$	Oxygen saturation constant	0.35	0.35	0.35	0.35	0.35	0.35	g_{O_2}/m^3
η_H	Reduction factor for $q_{S,H,max}$ in anoxic conditions (denitrification)	—	—	—	—	0.5	0.5	—
K_{NO_2},H	Nitrite saturation constant in anoxic conditions	—	—	—	—	0.3	0.3	g_N/m^3
K_{NO_3},H	Nitrate saturation constant in anoxic conditions	—	—	—	—	0.3	0.3	g_N/m^3
Ammonia oxidizing bacteria (AOB)								
$\mu_{AOB,max}$	Maximum specific growth rate	—	—	—	—	0.5	0.5	1/day
b_{AOB}	Decay rate constant	—	—	—	—	0.01	0.01	1/day
K_{O_2},AOB	Oxygen saturation constant	—	—	—	—	0.01	0.01	g_{O_2}/m^3
K_{NH_3},AOB	Ammonia saturation constant	—	—	—	—	0.07	0.07	g_N/m^3
Nitrite oxidizing bacteria (NOB)								
$\mu_{NOB,max}$	Maximum specific growth rate	—	—	—	—	0.5	0.5	1/day
b_{NOB}	Decay rate constant	—	—	—	—	0.01	0.01	1/day
K_{O_2},NOB	Oxygen saturation constant	—	—	—	—	0.02	0.02	g_{O_2}/m^3
K_{NO_2},NOB	Nitrite saturation constant	—	—	—	—	0.05	0.05	g_N/m^3

DOI 10.1002/bit

Mass transfer								
D_{O_2}	Diffusivity of oxygen	2×10^{-4}	2×10^{-4}	2×10^{-4}	2×10^{-4}	2×10^{-4}	2×10^{-4}	m^2/day
D_S	Diffusivity of substrate	1×10^{-4}	1×10^{-4}	1×10^{-4}	1×10^{-4}	1×10^{-4}	1×10^{-4}	m^2/day
D_{NH_3}	Diffusivity of ammonia	—	—	—	—	1×10^{-4}	1×10^{-4}	m^2/day
D_{NO_2}	Diffusivity of nitrite	—	—	—	—	1×10^{-4}	1×10^{-4}	m^2/day
D_{NO_3}	Diffusivity of nitrate	—	—	—	—	1×10^{-4}	1×10^{-4}	m^2/day
L_L	Mass transfer boundary layer thickness	60	60	60	60	60	60	μm
k_{det}	Biomass detachment velocity constant	416	104	1400	0	200	200	$m^{-1}day^{-1}$
f_{ata}	Fraction re-attached cells	—	—	—	—	0.2	0.2	—
Computational parameters								
$m_{X,max}$	Maximum cell mass (all biomass types)	2×10^{-12}	2×10^{-12}	5.36×10^{-11}	5.36×10^{-11}	2×10^{-12}	2×10^{-12}	$g_{COD,X}$
$L_X \times L_Z$ ($\times L_Y$)	System size	400×400	400×400	$400 \times 400 \times 400$	$400 \times 400 \times 400$	400×400	400×400	μm×μm(×μm)
$I \times K$ ($\times J$)	Number of discretization grid nodes	129×129	129×129	$65 \times 65 \times 65$	$65 \times 65 \times 65$	129×129	129×129	

Parameter values used in certain simulations are indicated with *1A2d*, *1B2d*, *1A3d*, and *1B3d* (for Case 1—biofilm consolidation example), and with *2A2d* and *2B2d* (for Case 2—colonies in EPS). *2d* means all two-dimensional and *3d* means all three-dimensional simulations.

In case *1A2d*, the concentrations of COD and O_2 in the bulk liquid are high enough to allow fast growth of biomass components in a flat and compact active layer just below the biofilm surface (Fig. 4A). Consequently, new biomass is uniformly introduced into the system a given height z, and gradients of pressure develop only perpendicular to the substratum. Figure 8 shows the cell positions and the biofilm surface at two moments in time. This illustrates how, due to the overall movement of the biofilm matrix, cells shift at higher advective speeds when situated closer to the nutrient source (biofilm surface here). Some of the cells situated near to the surface will detach (cells in contour B on Fig. 8), other new cells can also attach (cells in contour A).

Experiments suggest two major mechanisms contributing to formation of a gradient in biofilm density: (i) biofilm consolidation depending on the biofilm age, and (ii) larger amount of inert material in older biofilms (Bishop et al., 1995; Ohashi et al., 1999; Staudt et al., 2004). The biomass profile plots B and C in Figure 4 show these trends. Two distinct regions can be observed in the biomass profiles: a dense base film from substratum up to about 60–80 μm and a distinctly lighter top layer extending above the base film. The first mechanism is based on the fact that the net EPS formation is the result of two opposite processes. In the top region, due to both COD and O_2 availability, there is an active biomass layer generating cells and EPS. This means creation of new biofilm volume and a negative pressure gradient in the z direction ($\partial p/\partial z < 0$). The result is in an upward biomass flow ($u_z > 0$), eventually leading to detaching biomass. Conversely, in the base region the organic substrate (COD) is depleted, which stops the EPS production rate. As a result, the still occurring EPS hydrolysis will lead to a net EPS consumption. When EPS is disappearing there is a potential loss in biofilm volume, which generates a positive pressure gradient ($\partial p/\partial z > 0$) and a biomass flow directed towards the substratum ($u_z < 0$). The intersection plane of the two regions is marked by a change of sign for the vectorial component of pressure gradient perpendicular to substratum. In this plane $\partial p/\partial z = 0$ and consequently, $u_z = 0$. In Figure 4A the intersection plane is shown by a white line. In the simulations, an increase in biomass density occurs in this thin region since cells are not transported away from here. This unstable equilibrium probably does not happen in reality, where other stochastic factors would perturb it. The second mechanism involves conversion of active biomass to inerts in the biofilm depth, where the main nutrients are not available. Figure 4B shows total biomass volume fraction equal to one ($\varepsilon_H + \varepsilon_I + \varepsilon_E = 1$), a normal value in this case when no water-filled voids formed in the biofilm. However, the inert fraction ε_I dominates the biofilm base, while the EPS fraction ε_E is severely reduced. The biomass density profile (Fig. 4C) clearly shows the consolidation effect. The base layer is denser (150 g/L) than the top layer (50–60 g/L), and the height of the base layer is continuously increasing in time. This case shows that the factor of time and the distribution of particulate components have indeed a large impact of consolidation.

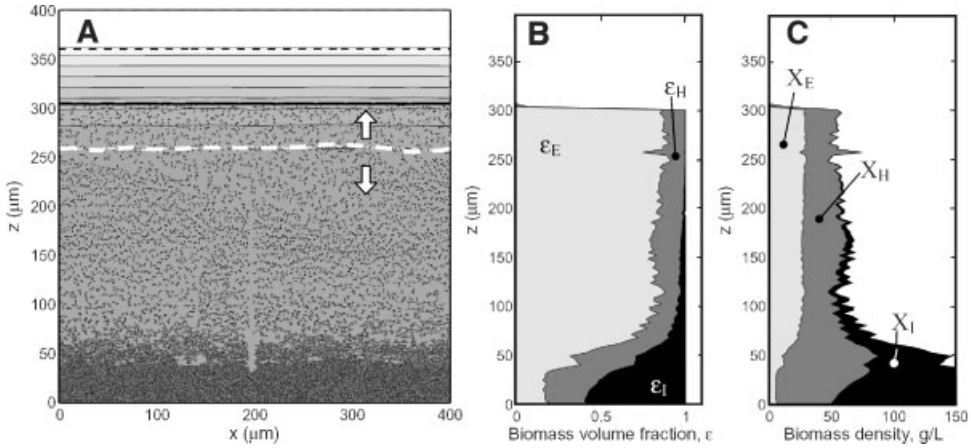

Figure 4. Example of 2-d simulation of a geometrically homogeneous biofilm development after 40 days (case *1A2d*—DO 4 g/m^3 and COD 100 g/m^3 in bulk liquid), showing the consolidation effect. **A**: 2-d distribution of dissolved oxygen, with thin contour lines and gray shades showing a gradual (contours at equal intervals) decrease in concentration from the highest value in the bulk liquid (white, 4 g/m^3) to the lowest (dark gray, <0.4 g/m^3). The top of the mass transfer boundary layer (MTBL) (95% O_2 concentration from the bulk liquid value) is displayed by a thick black dashed curve. The biofilm surface is shown by a thick continuous black curve. The white dashed line in the biofilm, at 50 μm from the biofilm surface, shows the zero biofilm advection velocity limit: above this line cells move upwards and below it cells move downwards. **B**: Profiles of average volume fractions of different biomass components along the biofilm depth: EPS (ε_E, light gray), active heterotrophic biomass (ε_H, dark gray), and inert biomass (ε_I, black). **C**: Profiles of average concentrations of different biomass components along the biofilm depth: EPS (X_E, light gray), active heterotrophic biomass (X_H, dark gray), and inert biomass (X_I, black).

Several modeling studies attempt to explain formation biofilm heterogeneity, that is, the ''fingering behavior'' (e.g., CA—Picioreanu et al., 1998; IbM—Kreft et al., 2001; continuum—Dockery and Klapper, 2001; Eberl et al., 2001). All these studies, based on nutrient diffusion/reaction coupled with biomass growth models, have shown that biofilm surface heterogeneity (''finger'' development) is enhanced by nutrient limitations. The model proposed here reflects the same behavior at low oxygen concentration in the bulk liquid, that is, in a *transport*-limited regime (case study *1B2d*). However, due to EPS decay, one more mechanism leading to surface heterogeneity is active here. At some moment in time, a small perturbation of the biofilm interface will come into contact with the negative (i.e., towards substratum) biomass flow field and a fast decay at this point will begin, as seen in Figure 6C. The explanation for biofilm consolidation in this simulation is twofold: (i) the impact from the heterogeneity of biofilm interface and (ii) the difference in volume fractions at the base and in the upper regions of the biofilm. The averaged volume fraction profile shows that the developing pore causes a decrease of total volume fraction at a height of circa 150 μm (Fig. 6D). Due to slower substrate transport, when the biofilm interface is heterogeneous the consolidation effect will be enhanced also for an even distribution of particulate components within the biomass. A significant consolidation effect is apparent in the profile plot of average density of particulates distribution along the direction perpendicular to substratum (Fig. 6F).

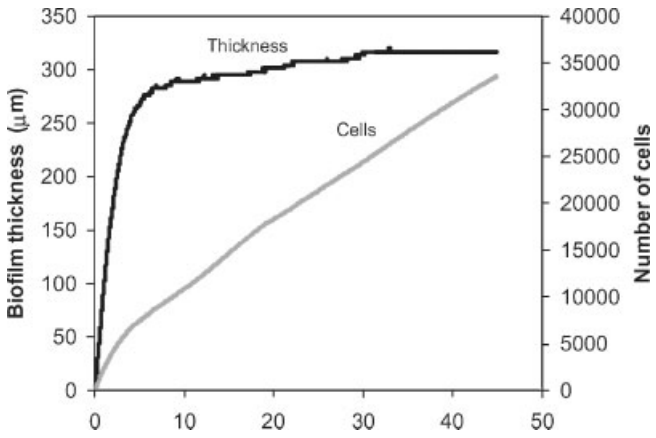

Figure 5. Time course of biofilm thickness (black) and number of biomass particles or cells (gray) in the case *1A2d* simulation, showing the consolidation effect.

The hybrid-continuum modeling framework was also implemented in a three-dimensional case. Simulation results from Figure 7 present a case where the biofilm surface develops in a stable way (i.e., relatively flat) (case study *1A3d*) and another case with unstable (i.e., irregular surface) biofilm/liquid interface (case study *1B3d*). Although quantitative differences exist (as pointed also in other studies by Eberl et al., 2001 and Picioreanu et al., 2004), the extra dimension does not introduce a significant change of the conclusions drawn from the 2-d simulations. The additional computational time is significant in 3-d, and it is a factor that may justify simulation studies to be performed preferentially using a 2-d setting, especially when only qualitative results are desired.

In particle-based models (Xavier et al., 2005a,b), the volume reduction due to cell and EPS decay or inactivation will generate empty spaces between particles. If biofilm shrinking is a desired model feature, then one possible mechanism to partially fill these voids is by moving neighboring particles together proportional to a distance equal to the reduction of particle radius (Xavier et al., 2005b). However, this technique is empirical, used solely for

DOI 10.1002/bit

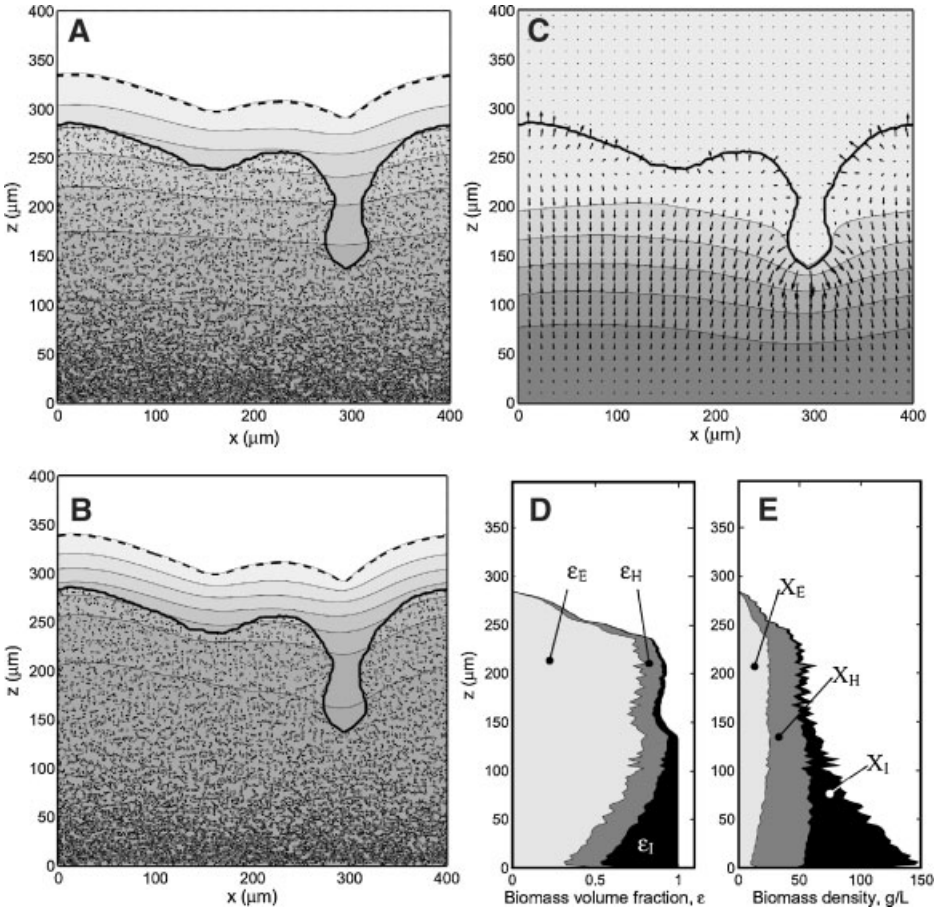

Figure 6. Example of 2-d simulation of a geometrically heterogeneous biofilm development after 45 days (case *1B2d*—at DO 1.5 g/m^3 and COD 1.5 g/m^3 in bulk liquid), showing the consolidation effect. **A**: 2-d distribution of dissolved oxygen concentration, with thin contour lines and gray shades showing a gradual decrease in concentration from the highest value in the bulk liquid (white) to the lowest (dark gray). The top of the oxygen MTBL (95% O_2 concentration from the bulk liquid value) is displayed by a thick dashed curve. The biofilm surface is shown by a thick continuous black curve. **B**: 2-d distribution of organic substrate concentration (as COD). The graph description is the same with that of panel (A). Contour lines are at equal intervals of concentration from 1.5 to 0.1 gO_2/m^3 and from 1.5 to 0.13 gCOD/m^3, respectively. **C**: 2-d distribution of pressure within the biofilm, with thin contour lines and gray shades showing a gradual decrease in pressure from the high values (light gray) in a narrow layer near the biofilm surface (the ''active layer'') to the lowest values in the biofilm depth (dark gray). Arrows display the vector field of biomass advective velocity generated by the pressure gradient. **D**: Profiles of average volume fractions of different biomass components along the biofilm depth: EPS (ε_E, light gray), active heterotrophic biomass (ε_H, dark gray), and inert biomass (ε_I, black). **E**: Profiles of average concentrations of different biomass components along the biofilm depth: EPS (X_E, light gray), active heterotrophic biomass (X_H, dark gray), and inert biomass (X_I, black).

computational convenience, and it is neither mathematically nor physically justified. For the hybrid-continuum modeling framework on the other hand, such techniques are not needed or used, as the pressure driven flow field will be moving particles in a continuum manner.

Case 2: Colonies Growing Embedded in an EPS Matrix

A large number of microscopy studies report on the spatial microbial distribution in nitrifying biofilms (e.g., Okabe et al., 2004; Satoh et al., 2004). It appears that a typical architectural model of such systems consists of compact clusters of autotrophic bacteria (i.e., nitrifiers) growing embedded in an EPS matrix presumably built by a heterotrophic biofilm component. An example of such a biofilm structure is shown in Figure 9.

To study colony formation in the EPS matrix, a biofilm system consisting of ammonia-oxidizing bacteria (AOB), nitrite-oxidizing bacteria (NOB), and heterotrophs, was modeled in the case further denoted as *2A2d*. Kinetics and stoichiometry of biological processes are presented in Table I. All nine biological processes were included in case *2A2d*. Parameters for this simulation are listed in Table II. The process description and the parameters for biological processes were set in analogy with the activated sludge models (ASM) (Henze et al., 2000). Moreover, we chose a simple process of direct EPS degradation to soluble substrate independent of the presence of cells. As little is known about EPS degradation, other assumptions may reflect better the reality, and these could be easily tested in future within the modeling framework presented here.

An example of biofilm structure progression in time is shown in Figure 10. Due to the EPS production, the

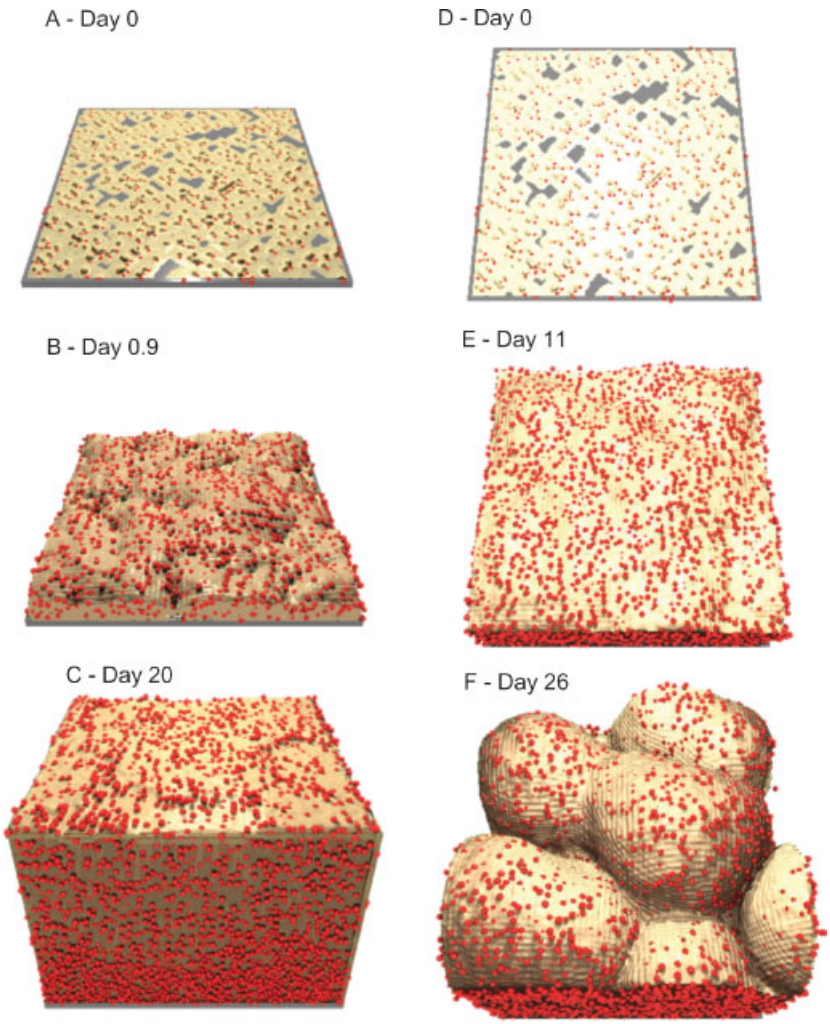

Figure 7. Examples of 3-d biofilm development simulations: (**A**–**C**) case *1A3d* (DO 4 g/m^3 and COD 100 g/m^3 in bulk liquid)—oxygen availability leading to a flat biofilm surface; (**D**–**F**) case *1B3d* (DO 0.5 g/m^3 and COD 100 g/m^3 in bulk liquid)—oxygen limitation leading to irregular biofilm surface. Heterotrophic bacteria are illustrated by red spheres and the EPS matrix by a light-yellow partially transparent surface. Biofilm height in panel C is 290 μm and in panel F is 235 μm. A higher density of cells can be seen at the base of the biofilm in panel C.

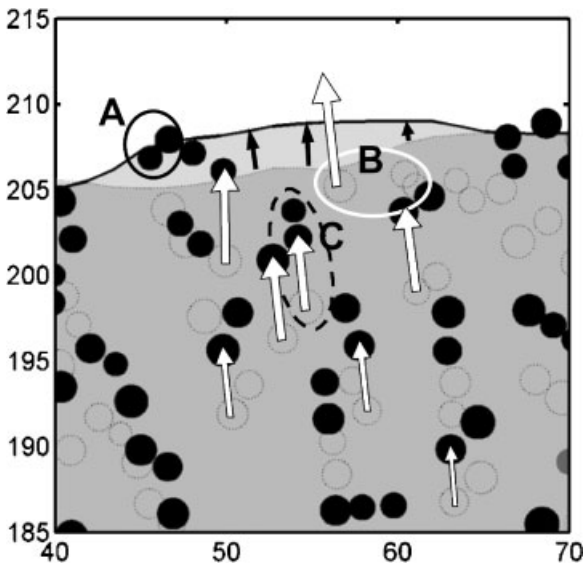

heterotrophic cells appear to move away from each other. This EPS matrix scattered with loose heterotrophs hosts colonies of AOB and NOB. The AOB and NOB, according to this model setup, do not produce EPS and tend to grow in compact clusters. The shape and size of these clusters depends on the biomass growth rate and position in the biofilm. First, the slower-growing NOB form rounder colonies than AOB. Due to a higher growth rate towards the biofilm top correlated also with a higher EPS volume production by heterotrophs, both inducing a higher advective velocity of the matrix, the AOB colonies are ''stretched''

Figure 8. Cell positions (circles) and EPS (gray area with a top boundary curve) at day 18 (dotted circles and dark gray EPS with dotted boundary line) are for comparison superimposed on those at day 18.25 (full circles and light gray EPS with continuous boundary line). Seven examples of cell displacement in this time interval are shown with white vector arrows. The black cells enclosed in the black ellipse (**A**) are newly incorporated biofilm cells coming by attachment. The cells enclosed in the white contour (**B**) are detached in this time interval. An example of cell division can be seen within the dashed contour (**C**).

DOI 10.1002/bit

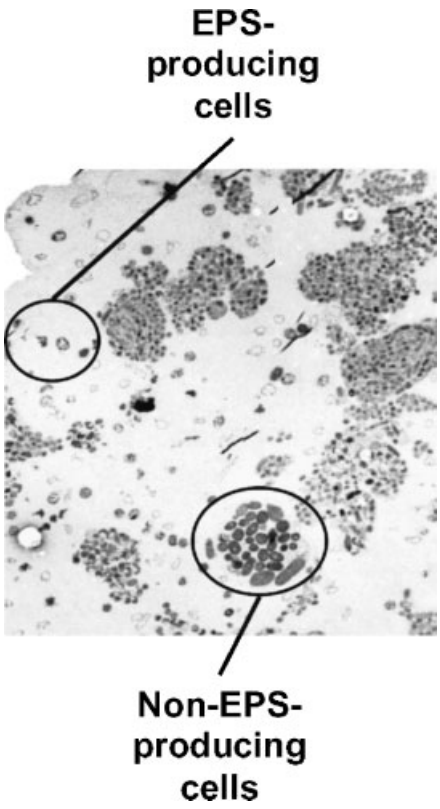

Figure 9. Compact colonies of aerobic nitrifying bacteria growing embedded in the EPS matrix presumably produced by heterotrophic bacteria scattered in the EPS volume. The microscopy image is of a biofilm growing on carrier particles in a biofilm air-lift suspension reactor (Tijhuis et al., 1995). The diameter of an individual non-EPS-producing cell from the colony shown in the circle is about 2 μm.

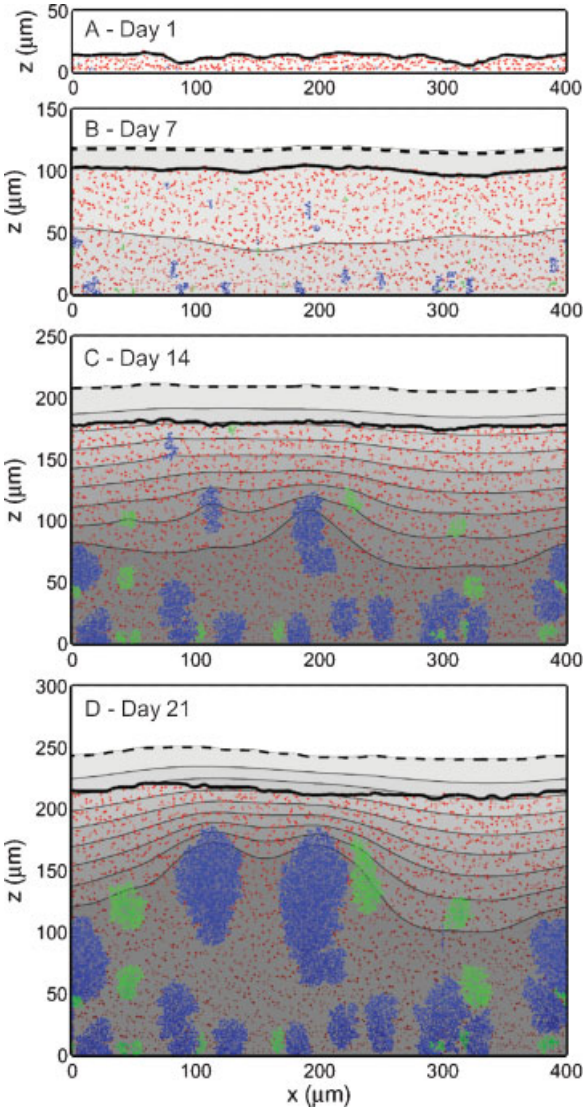

Figure 10. Example of 2-d microbially heterogeneous biofilm development at different moments in time (case *2A2d*—DO 10 g/m^3, COD 100 g/m^3, N-NH_3 10 g/m^3 in bulk liquid), for top-down biofilm aeration. Red dots are heterotrophic bacteria, blue are ammonia-oxidizing bacteria (AOB), and green are the nitrite-oxidizing bacteria (NOB). The color of bacteria gradually becomes darker as the cells get inactive. Two-d distribution of dissolved oxygen (DO) concentration is displayed on the background of each panel. Thin contour lines and gray shades show a gradual decrease in DO from the highest value in the bulk liquid (white) to the lowest (dark gray). The iso-concentration lines are at equal intervals of concentration from 10 to 0 gO_2/m^3. The top of the oxygen MTBL (95% O_2 concentration from the bulk liquid value) is represented by a thick dashed curve. The biofilm surface is shown by a thick continuous black curve.

accordingly, and transformed into ellipsoidal shaped colonies. The roundness of colonies towards the substratum is therefore also due to a lack of EPS production at the bottom. Second, higher nutrient availability at the biofilm top leads to larger colonies in upper biofilm zones. This variation on colony size is in line with the experimental results by Okabe et al. (2004). Third, the AOB and NOB towards the biofilm bottom continue to grow in round colonies in an EPS matrix originally created by heterotrophs. The heterotrophs present in the biofilm depth at day 21 stop being active due to lack of oxygen (Fig. 10D) or organic substrate (Fig. 11B), although nitrite and nitrate for denitrification were still available (Fig. 11C and D). Because the largest contribution to the advective biomass flow is due to heterotrophic grow with EPS production, the AOB/NOB colonies will not take the elongated shape forming in the upper layer. Fourth, there are less NOB than AOB due to differences in growth yield and due to reduced nitrite availability. Because the nitrite concentration in the bulk liquid was set to zero, the only nitrite available for NOB comes via diffusion from the AOB colonies. There are places where nitrite is produced (AOB colonies) and places where it is consumed (NOB colonies and denitrifying heterotrophs), leading to very important concentration gradients in all spatial directions (as shown also in Picioreanu et al., 2004). Fifth, the model shows considerable decay within the AOB and NOB colonies, a detail experimentally investigated by Leenen et al. (1997), but with consequences that remain to be further evaluated. In this case, the gradient in NOB decay rate is correlated with less nitrite availability towards the colony center (Fig. 11E) or with the presence of AOB colonies in the neighborhood (Fig. 11F). Summarizing, the colonies of NOB situated closer to AOB appear to grow bigger and produce more nitrate

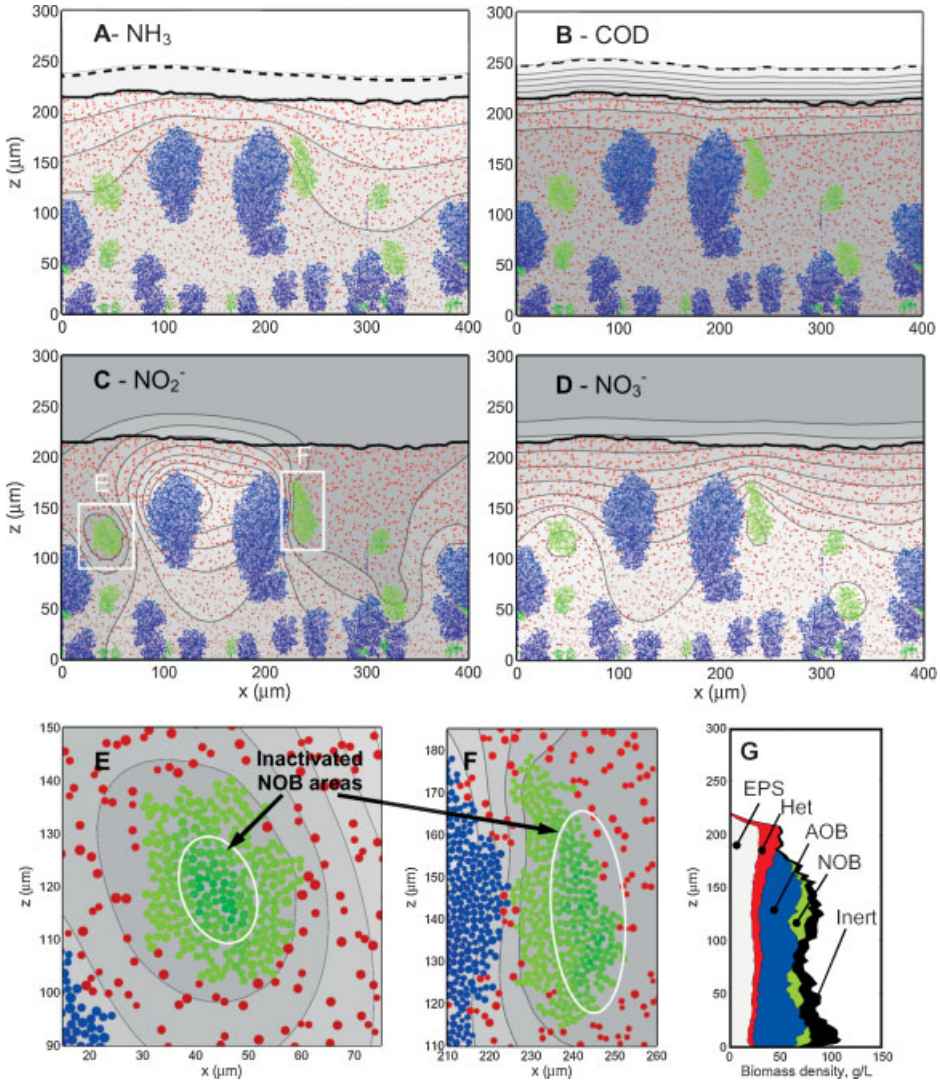

Figure 11. Two-d distributions of NH_3 (**A**), substrate as COD (**B**), nitrite (**C**) and nitrate (**D**) after 21 days, simulated for the system case *2A2d* (DO 10 g/m^3, COD 100 g/m^3, N-NH_3 10 g/m^3 in bulk liquid), for top-down biofilm aeration. White areas in the contour plots represent the highest concentrations, gradually changing to dark gray for the lowest concentrations. Iso-concentration lines are at equal intervals of concentration between 10 and 5.6 gN-NH_3/m^3, 3 and 0.02 gCOD/m^3, 0.8 and 0 gN-NO_2/m^3, 3.6 and 0 gN-NO_3/m^3. The biofilm surface is shown by a thick continuous black curve. Red dots are heterotrophic bacteria, blue are ammonia-oxidizing bacteria (AOB), and green are the nitrite-oxidizing bacteria (NOB). The color of bacteria gradually becomes darker as the cells get inactive. **E**: Detail from **panel C** showing less active NOB (darker green cells) in the middle of a colony. **F**: Detail from (C) showing less active NOB cells at the side not in contact with the AOB colony (blue cells). **G**: Profiles of average concentrations of different biomass components along the biofilm depth: EPS (X_E, light gray), active heterotrophic biomass (X_H, red), active AOB (X_{AOB}, blue), active NOB (X_{NOB}, green), and inert biomass (X_I, black).

although they are at the same depth in the biofilm (see examples in Fig. 11D).

The growth of nitrifying biofilms in membrane aerated biofilm reactors (MABR; Hibiya et al., 2003; Pankhania et al., 1994) can also be easily studied. In this case (*2B2d*), the only modification needed is a boundary condition with fixed value for oxygen concentration at the biofilm/membrane surface. Concentrations of oxygen at the membrane side and in the bulk liquid were set at 10 and 1 g/m^3, respectively. Several advantageous characteristics of MABR systems over conventional biofilm reactors, as pointed out by Satoh et al. (2004), are clearly revealed in the model simulations presented in Figure 12. First, nitrifying bacteria in the MABR are immobilized in the deeper parts of the biofilm, where they experience high O_2 concentrations (Fig. 12E) while organic carbon concentration is low (Fig. 12B). In the conventional top-down aeration, autotrophic nitrifying bacteria are excluded from the upper aerobic layer of the biofilm due to the faster growth of heterotrophic bacteria. Second, after the same time of biofilm development, NOB and AOB colonies are bigger in the membrane aeration case than in the normal aeration, observation also in line with Satoh et al. (2004). Third, the AOB grow faster in the middle of the 220 µm thick biofilm, and their inactivation is more pronounced both towards the biofilm top and towards the bottom (Fig. 12F compared with Fig. 11G). At the same time, the nitrite concentration appears to be higher in the middle of the biofilm (Fig. 12C).

DOI 10.1002/bit

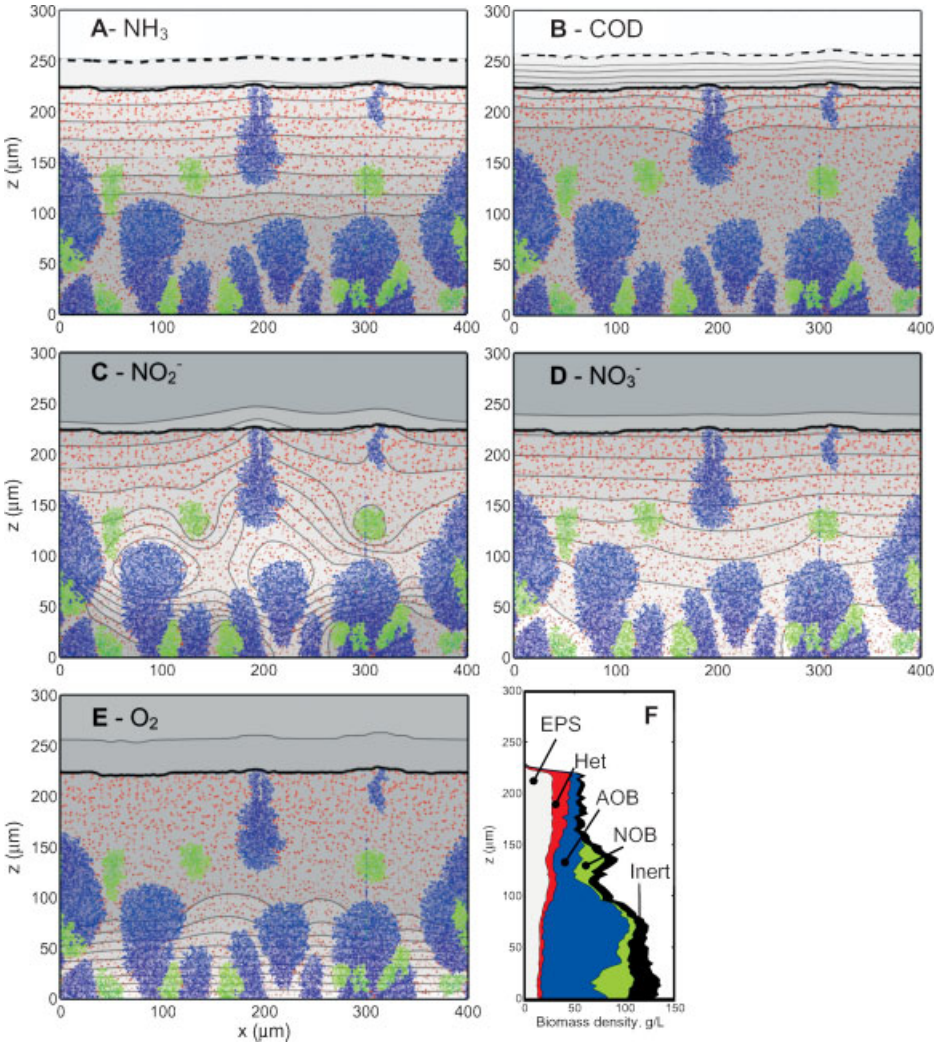

Figure 12. Two-d distributions of NH3 (**A**), substrate as COD (**B**), nitrite (**C**), nitrate (**D**), and oxygen (**E**) after 21 days, simulated for the system case *2B2d* (DO 1 g/m^3, COD 100 g/m^3, N-NH_3 10 g/m^3 in bulk liquid), with membrane aeration (DO 10 g/m^3 on membrane side). Plot descriptions are as for Figure 11. Iso-concentration lines are at equal intervals of concentration between 10 and 0 gN-NH_3/m^3, 3 and 0.04 gCOD/m^3, 1.4 and 0 gN-NO_2/m^3, 10.1 and 0 gN-NO_3/m^3, 10 and 0.05 gO_2/m^3. **F**: Profiles of average concentrations of different biomass components along the biofilm depth: EPS (X_E, light gray), active heterotrophic biomass (X_H, red), active AOB (X_{AOB}, blue), active NOB (X_{NOB}, green), and inert biomass (X_I, black).

CONCLUSIONS

An innovative type of biofilm model was derived and evaluated within this study. This model is the first of its kind introducing a combination of two previously very different approaches in biofilm modeling: a continuum representation of EPS and a discrete individual description of microbial cells. The hybrid model retains the advantages of each approach while providing more realistic descriptions of biofilm structure dynamics in two or three spatial dimensions.

One model application describes the consolidation effect present in mature biofilms. Modeling results suggest that the governing process behind biofilm consolidation is the presence of a negative pressure in the lower region of the biofilm, generated by EPS and cell degradation processes. The pressure gradients may lead to biofilm volume shrinking, with cell transport towards the substratum. This mechanism can explain the formation of a denser layer of cells in the biofilm depth. Two- and three-dimensional model simulations show the same trend. Occurrence of other known structural characteristics, such as formation of an irregularly shaped biofilm surface under nutrient limiting conditions, was also apparent from the simulations. Another apparent advantage of the hybrid continuum-discrete model is in the biofilm shrinking mechanism based on a rigorously defined contractive pressure, in turn generated by the decay-driven volume loss. Unlike in pure particle-based models, biofilm contraction does not need special computational attention, having the same mechanism as the growth driven biomass transport. Moreover, biofilm detachment can be included easier in the continuum biofilm matrix representation than in the particle-based models.

A second model application explains formation of autotrophic microbial colonies in the EPS matrix produced by heterotrophic cells. The model shows how the shape and size of autotrophic colonies embedded in the EPS develop as

a function of nutrient availability. The importance of considering multi-dimensional gradients and fluxes of intermediate metabolic components such as nitrite is revealed. The advantages of using a membrane-aeration system over the normal top-down biofilm aeration in simultaneous C/N removal are outlined.

In order to refine this type of computational biofilm models, it is becoming important to perform experiments revealing a series of missing data regarding EPS behavior. Mechanical properties of EPS (e.g., elasticity, viscosity, and other flow characteristics), kinetics of EPS formation in biofilms, and how EPS production is regulated are only a few topics that will need special attention.

Animations of the simulations presented in this article can be downloaded from our web site at http://www.biofilms.bt.tudelft.nl/continuumEPS_discreteCells/index.html. The computer program used as framework for building the specific biofilm models used in this study will be made available at the same web site.

NOTATIONS

b_i	Decay rate coefficient for a particulate component i, 1/T
C	Concentration of soluble or particulate component, M/L^3
D_i	Diffusion coefficient of a soluble component i, L^2/T
h	Spatial discretization step, L
I, J, K	Number of grid nodes in the spatial discretization
$\mathbf{j}$	Mass flux of a soluble or particulate component, M/L^{2}T
$\mathbf{j}_S$	Mass flux of a soluble component, M$_S$/L^{2}T
$\mathbf{j}_X$	Mass flux of a particulate component, M$_X$/L^{2}T
f_{ata}	Fraction of attached to detached cells
k_{det}	Biomass detachment rate coefficient, 1/(LT)
$K_{i,j}$	Saturation (Monod) constant for a soluble component i for a biomass component j, M$_{S,i}$/L^3
L_F	Maximum biofilm thickness, L
L_L	Mass transfer boundary layer thickness, L
m_0	Initial mass of a biomass particle, M$_X$
$m_{X,i,P}$	Biomass of type i contained in the spherical particle p, M$_{X,i}$
$m_{X,P}$	Total biomass contained in the spherical particle p, M$_X$
$m_{X,max}$	Maximum biomass contained in the spherical particle p, M$_X$
n_P	Number of spherical biomass particles (microbial cells)
$n_{X,i,0}$	Number of initial biomass particles (microbial cells) of each type i
n_S	Number of soluble components
n_X	Number of particulates components (biomass types)
N	Number of grid nodes in the temporal discretization
p	Biomass pressure, M/LT^2
$q_{S,H,max}$	Maximum specific substrate uptake rate by heterotrophic biomass, M$_S$M$_X$/T
r	Net production rate of a soluble or particulate component, M/L^{3}T
$r_{S,i}$	Net production rate of a soluble component i, M$_{S,i}$/L^{3}T
$r_{X,i}$	Net production rate of a particulate component i, M$_{X,i}$/L^{3}T
$r_{X,E}$	Net production rate of EPS, M$_E$/L^{3}T
R_P	Radius of a biomass particle, L
$R_{P,0}$	Initial radius of a biomass particle, L
R_X	Global rate of biofilm volume generation, 1/T
L_X, L_Y, L_Z	Dimensions of the computational domain, L
S_i	Concentration of a soluble component i, M$_{S,i}$/L^3
$S_{B,i}$	Concentration of a soluble component i in the bulk liquid, M$_{S,i}$/L^3
t	Time, T
$\mathbf{u}$	Global advection speed in the biofilm, L/T
$\mathbf{u}_{cell}$	Composite velocity of cells movement, L/T
$\mathbf{u}_{shov}$	Speed of cells displacement due to shoving, L/T
u_{det}	Detachment velocity at the biofilm surface, L/T
x, y, z	Spatial coordinates, L
X_i	Concentration of a particulate component (per biofilm volume), M$_{X,i}$/L^3
X_E	Concentration of EPS (per biofilm volume), M$_E$/L^3
Y_i	Yield of a biomass type on a certain substrate, M$_{X,i}$M$_{S,i}$
ε_i	Volume fraction of biomass type i in biofilm, L$_i^3$/L^3
ε_E	Volume fraction of EPS in biofilm, L$_E^3$/L^3
ϕ	Level-set function
Γ_B	Bulk liquid boundary
Γ_{LF}	Biofilm-liquid boundary (biofilm surface)
Γ_{BL}	Top boundary of the mass transfer boundary layer
Γ_P	Periodic lateral boundaries
Γ_S	Substratum boundary
η	Dynamic viscosity of biofilm fluid model, M/LT
λ	Darcy's law parameter, L^{3}T/M
$\mu_{i,max}$	Maximum specific growth rate of a biomass type, 1/T
$\rho_{X,i}$	Density of biomass type i in a particle (per particle volume), M$_{X,i}$/L^3
$\rho_{X,E}$	Density of EPS in biofilm, M$_{EPS}$/L^3
τ	Time step, T
τ_w	Shear stress at the biofilm surface, M/LT^2
Ω_B	Bulk liquid sub-domain
Ω_F	Biofilm sub-domain
Ω_L	Mass transfer boundary layer

Indices i may refer either to soluble components O_2 = dissolved oxygen, S = organic substrate (as COD), NH_3 = ammonia+ammonium, NO_2 = nitrite+HNO_2, NO_3 = nitrate or to biomass components E = EPS, I = inert biomass, H = heterotrophs, AOB = ammonium oxidizing bacteria, and NOB = nitrite oxidizing bacteria (see also Table II).

Erik Alpkvist acknowledges the financial support of the KK foundation and the scientific assistance of Dr. Magnus Christensson from AnoxKaldnes AB. The authors thank Dr. Jan-Ulrich Kreft from the University of Bonn for very carefully reading this manuscript and Dr. Joao Xavier from Universidade Nova de Lisboa for the useful discussions and comments.

References

Alpkvist E. 2005. Modelling and simulation of heterogeneous biofilm growth using a continuum approach. Licentiate thesis in mathematical sciences, Lund University, Sweden (ISBN 91-631-6871-5).

Bishop PL, Zhang TC, Fu YC. 1995. Effects of biofilm structure, microbial distributions and mass-transport on biodegradation processes. Water Sci Technol 31(1):143–152.

Brandt A. 1977. Multi-level adaptive solutions to boundary value problems. Math Comp 31(138):333–390.

De Beer D, Stoodley P, Roe F, Lewandowski Z. 1994. Effects of biofilm structures on oxygen distribution and mass transport. Biotechnol Bioeng 43:1131–1138.

Dockery J, Klapper I. 2001. Finger formation in biofilm layers. SIAM J Appl Math 62(3):853–869.

Eberl HJ, Picioreanu C, Heijnen JJ, Van Loosdrecht MCM. 2000. A three-dimensional numerical study on the correlation of spatial structure, hydrodynamic conditions, and mass transfer and conversion in biofilms. Chem Eng Sci 55:6209–6222.

Eberl HJ, Parker DF, Van Loosdrecht MCM. 2001. A new deterministic spatio-temporal continuum model for biofilm development. J Theor Med 3:161–175.

DOI 10.1002/bit

Glasbey CA, Horgan GW. 1994. Image analysis for the biological sciences. Chichester UK: John Wiley & Sons. pp 128–137.

Henze M, Gujer W, Mino T, Van Loosdrecht MCM. 2000. Activated sludge models ASM1, ASM2, ASM2d and ASM3. IWA Scientific & Technical Report, IWA Publishing, London, UK.

Hibiya K, Terada A, Tsuneda S, Hirata A. 2003. Simultaneous nitrification and denitrification by controlling vertical and horizontal microenvironment in a membrane-aerated biofilm reactor. J Biotechnol 100:23–32.

Jiang G, Peng D. 2000. Weighted ENO schemes for Hamilton-Jacobi equations. SIAM J Sci Comput 21(6):2126–2143.

Klapper I, Rupp CJ, Cargo R, Purvedorj B, Stoodley P. 2002. Viscoelastic fluid description of bacterial biofilm material properties. Biotechnol Bioeng 80(3):289–296.

Kreft J-U. 2004. Biofilms promote altruism. Microbiology-SGM 150:2751–2760.

Kreft J-U, Booth G, Wimpenny JWT. 1998. BacSim, a simulator for individual-based modelling of bacterial colony growth. Microbiology-SGM 144:3275–3287.

Kreft J-U, Wimpenny JWT. 2001. Effect of EPS on biofilm structure and function as revealed by an individual-based model of biofilm growth. Water Sci Technol 43(6):135–141.

Kreft J-U, Picioreanu C, Wimpenny JWT, Van Loosdrecht MCM. 2001. Individual-based modelling of biofilms. Microbiology-SGM 147: 2897–2912.

Kwok WK, Picioreanu C, Ong SL, van Loosdrecht MCM, Ng WJ, Heijnen JJ. 1998. Influence of biomass production and detachment forces on biofilm structures in a biofilm airlift suspension reactor. Biotechnol Bioeng 58(4):400–407.

Laspidou CS, Rittmann BE. 2004. Modeling the development of biofilm density including active bacteria, inert biomass, and extracellular polymeric substances. Water Res 38(14–15):3349–3361.

Leenen EJTM, Boogert AA, Van Lammeren AAM, Tramper J, Wijffels RH. 1997. Dynamics of artificially immobilized nitrosomonas europaea: Effect of biomass decay. Biotechnol Bioeng 55(4):630–641.

Manz B, Volke F, Goll D, Horn H. 2003. Measuring local flow velocities and biofilm structure in biofilm systems with magnetic resonance imaging (MRI). Biotechnol Bioeng 84(4):424–432.

Neu TR, Lawrence JR. 1997. Development and structure of microbial biofilms in river water studied by confocal laser scanning microscopy. FEMS Microbiol Ecol 24(1):11–25.

Ohashi A, Koyama T, Syutsubo K, Harada H. 1999. A novel method for evaluation of biofilm tensile strength resisting to erosion. Water Sci Technol 39(7):261–268.

Okabe S, Kindaichi T, Ito T, Satoh H. 2004. Analysis of size distribution and areal cell density of ammonia-oxidizing bacterial microcolonies in relation to substrate microprofiles in biofilms. Biotechnol Bioeng 85(1):86–95.

Pankhania M, Stephenson T, Semmens MJ. 1994. Hollow fibre bioreactor for wastewater treatment using bubbleless membrane aeration. Water Res 28(10):2233–2236.

Picioreanu C, Van Loosdrecht MCM. 2003. Use of mathematical modelling to study biofilm development and morphology. In: Lens P et al, editors. Biofilms in medicine, industry and environmental biotechnology—Characteristics, analysis and control. UK: IWA Publishing. pp 413–437.

Picioreanu C, Van Loosdrecht MCM, Heijnen JJ. 1998. Mathematical modeling of biofilm structure with a hybrid differential discrete cellular automaton approach. Biotechnol Bioeng 58(1):101–116.

Picioreanu C, Van Loosdrecht MCM, Heijnen JJ. 1999. Discrete-differential modelling of biofilm structure. Water Sci Technol 39(7):115–122.

Picioreanu C, Van Loosdrecht MCM, Heijnen JJ. 2000a. A theoretical study on the effect of surface roughness on mass transport and transformation in biofilms. Biotechnol Bioeng 68:354–369.

Picioreanu C, Van Loosdrecht MCM, Heijnen JJ. 2000b. Effect of diffusive and convective substrate transport on biofilm structure formation: A two-dimensional modeling study. Biotechnol Bioeng 69:504–515.

Picioreanu C, Van Loosdrecht MCM, Heijnen JJ. 2001. Two-dimensional model of biofilm detachment caused by internal stress from liquid flow. Biotechnol Bioeng 72(2):215–218.

Picioreanu C, Kreft J-U, Van Loosdrecht MCM. 2004. Particle-based multidimensional multispecies biofilm model. Appl Environ Microbiol 70(5):3024–3040.

Press WH, Teukolsky SA, Vetterling WT, Flannery BP. 1997. Numerical recipes in C: The art of scientific computing. New York: Cambridge University Press.

Satoh H, Ono H, Rulin B, Kamo J, Okabe S, Fukushi K-I. 2004. Macroscale and microscale analyses of nitrification and denitrification in biofilms attached on membrane aerated biofilm reactors. Water Res 38:1633–1641.

Sethian JA. 1996. A fast marching level set method for monotonically advancing fronts. Proc Nat Acad Sci USA 93(4):1591–1595.

Sethian JA. 1999. Fast marching methods. SIAM Rev 41(2):199–235.

Staudt C, Horn H, Hempel DC, Neu TR. 2004. Volumetric measurements of bacterial cells and extracellular polymeric substance glycoconjugates in biofilms. Biotechnol Bioeng 88(5):585–592.

Stoodley P, Lewandowski Z, Boyle JD, Lappin-Scott HM. 1999. Structural deformation of bacterial biofilms caused by short-term fluctuations in fluid shear: An in situ investigation of biofilm rheology. Biotechnol Bioeng 65:83–92.

Tijhuis L, Huisman JL, Hekkelman HD, Van Loosdrecht MCM, Heijnen JJ. 1995. Formation of nitrifying biofilms on small suspended particles in airlift reactors. Biotechnol Bioeng 47(5):585–595.

Wanner O, Gujer W. 1986. A multispecies biofilm model. Biotechnol Bioeng 28:314–328.

Wanner O, Eberl HJ, Morgenroth E, Noguera DR, Picioreanu C, Rittmann BE, Van Loosdrecht MCM. 2005. Mathematical modeling of biofilms. IWA Scientific and Technical Report no 18. UK: IWA Publishing.

Wood BD, Whitacker S. 1999. Cellular growth in biofilms. Biotechnol Bioeng 64:656–670.

Xavier JB, Picioreanu C, Van Loosdrecht MCM. 2005a. A framework for multidimensional modelling of activity and structure of multispecies biofilms. Environ Microbiol 7(8):1085–1103.

Xavier JB, Picioreanu C, Van Loosdrecht MCM. 2005b. A general description of detachment for multidimensional modelling of biofilms. Biotechnol Bioeng 91(6):651–669.